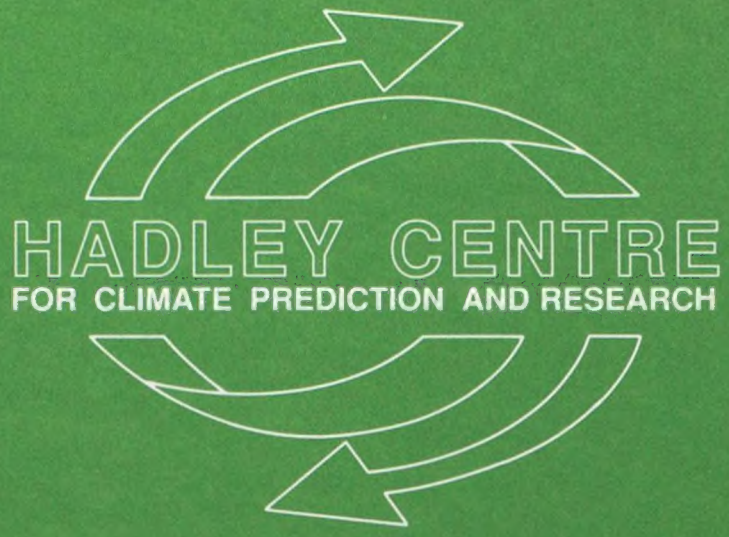

A GCM simulation of the impact of Amazonian deforestation on climate using an improved canopy representation.

by

J. Lean and P. R. Rowntree

CRTN 26 March 1992

CLIMATE
RESEARCH
TECHNICAL
NOTE

Hadley Centre
Meteorological Office
London Road
Bracknell
Berkshire RG12 2SY

CLIMATE RESEARCH TECHNICAL NOTE NO. 26

A GCM SIMULATION OF THE IMPACT OF AMAZONIAN DEFORESTATION ON CLIMATE USING AN IMPROVED CANOPY REPRESENTATION

by

J LEAN and P R ROWNTREE

Submitted for publication

Hadley Centre for Climate Prediction and Research
Meteorological Office
London Road
Bracknell
Berkshire RG12 2SY
U.K.

Note: This paper has not been published. Permission to quote from it should be obtained from the Director of the Hadley Centre.

Summary

To obtain a good estimate of the impact of Amazonian deforestation on local climate it is critical that the representation of the forest canopy within General Circulation Models (GCMs) is as realistic as possible. Recent measurements from the Amazonian forest have highlighted major weaknesses in our GCM simulation of the interception of rainfall from the forest canopy. Here, we present results for Amazonia from a new 3-year control experiment which incorporates an improved representation of micrometeorological processes within the forest. A detailed assessment of the control simulation reveals that the GCM provides a realistic description of the climate of Amazonia. In determining the impact of Amazonian deforestation on climate we present a comprehensive analysis of the simulated climate following the replacement of Amazonian forest by pasture. Results suggest a reduction in rainfall (14%) and evaporation (24%) and a rise in surface temperature (2°C) over the local area. Explanations are put forward to explain these changes.

1. Introduction

In the last two decades GCMs have been used to address the climatic consequences of one of the most serious threats to the global environmental system, namely tropical deforestation. Three recent GCM experiments, to assess the likely impact of Amazonian deforestation on climate (Dickinson and Henderson-Sellers 1988; Lean and Warrilow 1989; Shukla et al. 1990) have improved the credibility of such experiments by incorporating a more physically realistic treatment of the land surface. The rationale of these experiments was to represent more satisfactorily the changes in vegetation/soil parameters and hydrology that accompany such land degradation. However, the applicability of the results obtained is uncertain since aspects of the simulated forested climate have been shown to be flawed (Dickinson 1989; Shuttleworth and Dickinson 1989).

The version of the UK Meteorological Office GCM used by Lean and Warrilow (1989) has since been verified against observational data from the Amazonian forest (Shuttleworth 1988a). This has identified key deficiencies in the simulation of a canopy description for tropical forest. This is particularly pertinent to studying possible climatic implications of deforestation as the forest canopy has an integral role to play in the land surface/atmosphere moisture exchange. The forest canopy intercepts rainfall and thus regulates the amount of water reaching the surface. The fraction of the canopy that is covered by water then has zero resistance to evaporation, and can evaporate water rapidly into the atmosphere. Evaporation from the dry parts of the canopy will be subjected to stomatal control as well as possibly being limited by available soil moisture.

Following on from this important validation exercise, we report here on the development of an improved canopy interception formulation which takes some account of the spatial variability of rainfall. Results will be presented from a three-year control experiment. Several aspects of the surface hydrology together with important atmospheric variables will be analyzed as it is recognised that deficiencies in atmospheric variables such as net radiation and rainfall may conceal improvements made to the treatment of the land surface (Dickinson 1991). The control simulation will be validated against a number of independent observations for Amazonia. To meet this aim, we will use some of the most up to date datasets.

In assessing the impact of tropical deforestation on climate we will focus on Amazonia as this region with its expansive forest accounting for some 25% of all tropical forests has an important influence on the atmospheric circulation. Precise evaluations of the fraction of Amazonian forest destroyed to date are disputed but typical values are modest. For example, Fearnside (1990) estimates that the area cleared by 1988 has amounted to some 8% of the total 5 million km^2. However, more alarming evidence suggests that explosive rates of clearing are taking place over vast areas of Amazonia, which could lead to total loss of the forest (eg. Fearnside 1990; Salati 1989).

In order to evaluate the climatic consequences of the complete removal of the Amazonian forest, a three-year GCM simulation has been carried out in which tropical forest and savannah were replaced

by pasture in South America, north of 30°S. In a detailed assessment of the results we will consider the influence of this land transformation on all aspects of local climate.

2. Description of the Model

The version of the Meteorological Office GCM used here is an atmospheric global model (Slingo et al. 1989) which uses the primitive equations to describe and predict the atmospheric variables of surface pressure, and temperature, and wind, and humidity at 11 levels between the surface and the top of the atmosphere. The 11 sigma layers (sigma is equal to the pressure divided by its surface value) are spaced unevenly in the vertical to allow for enhanced resolution near the surface and in the upper troposphere. The horizontal resolution at each level is 2½° x 3¾°. The sea surface temperatures are prescribed as the model is run without an interactive ocean; these are taken from climatological values and are updated every 5 days.

Sub-grid scale processes are treated as follows. Radiative processes are computed interactively every three model hours. The radiation scheme computes diurnally and seasonally varying solar radiation. Both longwave and shortwave radiation interact with model diagnosed cloud, which has fixed optical properties. A cloud water variable has now been included and large-scale rainfall is diagnosed from the rate of depletion of cloud water (Smith 1990). A mass flux convection scheme (described in Gregory and Rowntree 1990) is included. The scheme uses a 'bulk' cloud model to represent an ensemble of convective clouds and aims to describe shallow, deep and mid-level convection. The number of model levels in the boundary layer is allowed to vary up to a maximum of four. Surface turbulent transfer of heat, moisture and momentum are calculated using Monin-Obhukhov similarity theory.

Geographical variation of land surface and soil types is represented within the model (Warrilow and Buckley 1989). The vegetation and soil types are based on the work of Wilson and Henderson-Sellers (1985). Their original 1° x 1° resolution primary and secondary vegetation and soil datasets were used to create spatially varying datasets of 17 soil and vegetation parameters which were interpolated onto the 2½° x 3¾° model grid (Warrilow and Buckley 1989). The vegetation parameters and soil parameters (as shown in Table 1) are specified globally in terms of locally derived parameters which were obtained from a review of the literature. Soil moisture concentration is defined as the ratio of the total volume of moisture to the total soil volume. Available soil moisture concentration is then the soil moisture concentration above a threshold value; this is the soil moisture concentration at wilting point, the point at which it becomes virtually impossible for plants to remove water from the soil. All parameters are derived at the start of a model experiment and are then assumed to be fixed throughout the run; that is the seasonal dependence of the parameters is ignored.

Details of all other aspects of the current land surface description are given in Warrilow et al. (1986). The surface hydrology scheme is characterised by a single soil moisture store. Following the important realisation that evaporation of rainfall intercepted by vegetation must be treated independently

of transpiration of water vapour (Shuttleworth and Calder 1979), a canopy is also represented. Precipitation is intercepted by the canopy and while the canopy remains wet, water vapour evaporates from the canopy at the potential or maximum rate. Bare soil is given a canopy capacity to represent ponding of water on a bare soil surface. Transpiration from the dry parts of the canopy and evaporation from the soil is subject to stomatal control and can be limited when the soil moisture concentration falls below a critical value. Water falling through the canopy onto the soil infiltrates into the soil at a rate equal to the saturated conductivity modified to take account of the presence of vegetation. When throughfall exceeds the infiltration rate the surplus of water runs off. Surface runoff takes account of spatial variations in rainfall by assuming that rainfall is only falling over a fraction of the grid box. Within this fractional area rainfall is assumed to be exponentially distributed. Sub-surface runoff is also diagnosed and is controlled by the gravitational drainage of soil moisture. Thermal processes are treated using a 4-layer soil temperature model.

3. Recent Improvements to the Model

Measurements, including dry-canopy evaporation and rainfall interception (the water that evaporates from the canopy without reaching the soil) from a tropical rainforest at a site in central Amazonia (Shuttleworth 1988a) have provided an unparalleled source of data with which to improve and validate the representation of micrometeorology within the model. In the light of this study we report on some recent developments to the representation of rainfall interception.

The objective of the 2-year intensive field campaign at Ducke Reserve, 25km from Manaus, Amazonas (Shuttleworth 1988a), was to use an empirically based micrometeorological model to obtain monthly values of total evaporation from the forest. Automatically collected values of standard meteorological variables were used to specify the parameters within the model. Measurements of the evaporation of intercepted rainfall (deduced as the difference between precipitation measured above the canopy and throughfall measured beneath) and dry canopy evaporation were used to calibrate the model.

In Figure 1 we compare monthly interception from a 3-year control experiment (OC) as presented in Lean and Warrilow(1989) with those values reported by Shuttleworth (1988a). It is apparent that the model significantly overestimates interception from September to April. This may be partially attributed to the assumption that precipitation falling onto the canopy does so uniformly over the whole of the grid square. Hence, the large spatial variability in rainfall over the area of a grid square, most prevalent during convective rain storms, is neglected. Another probable source of error is the value of 2.5mm chosen for the maximum amount of water that the canopy can hold and now measured as 0.74mm in the Amazonian forest (Lloyd et al. 1988).

A more realistic formulation was devised (Dolman and Gregory 1990) based on the work of Shuttleworth (1988b) which is more consistent with Warrilow's (1986) treatment of surface runoff. Rainfall that is intercepted by the canopy is assumed to fall over a fractional area μ of the total area of

the grid square. Within this area the distribution of rainfall is governed by a probability distribution function such that

$$f(R_L)=\frac{\mu}{R}\exp\left(\frac{-\mu R_L}{R}\right) \quad (1)$$

where $f(R_L)$ is the probability that rainfall exceeds R_L

R_L is the local rainfall rate

R is the grid average rainfall rate

μ is the proportion of the grid square over which rain falls

As water falls onto the canopy some will be captured and the rest will fall through to the surface. The local throughfall rate is defined as

$$TF_L=R_L\frac{C}{C_M} \quad (2)$$

where C is the canopy water content and C_M is the maximum amount of water that the canopy can hold. This formulation differs slightly from that suggested by Shuttleworth (1988b) in that throughfall occurs before the canopy is saturated as this is felt to be more realistic (Gregory personal communication 1990). Equation 2 is only applicable if the local canopy is not completely filled by the amount of water intercepted in a timestep Δt. If more water is intercepted during the timestep than it is possible for the local canopy to hold then the excess water is added to the throughfall and

$$TF_L=R_L-\left(\frac{C_M-C}{\Delta t}\right) \quad (3)$$

The throughfall averaged over the grid box is

$$TF=R\left(1-\frac{C}{C_M}\right)\exp\left(-\mu\frac{C_M}{R\Delta t}\right)+R\frac{C}{C_M} \quad (4)$$

The fractional area μ was set to 0.1 and 0.5 for convective and large-scale rainfall respectively. These values were derived from geometrical considerations (Eagleson and Qinliang 1985).

The model was modified to include the formulation as described above together with a reduced canopy capacity equal to the measured value of 0.74mm and a new control integration was run for three years (NC). In the following section the performance of this new control simulation NC is assessed.

4. Assessment of the New Control Simulation

In this section a comparison will be made between some important climatological variables from the new 3-year control integration NC, the old 3-year integration OC and observations for Amazonia. This will enable a thorough assessment of the impact of the new canopy formulation together with an assessment of how well the new integration captures reality and in turn how much confidence we should place in the modelled impact of deforestation on climate.

The observations presented in this section represent both climatological averages and data from the 2-year campaign in central Amazonia (Shuttleworth 1988a). More emphasis will be placed on good climatological data obtained from long-term meteorological measurements at one or more sites as these observations provide a better estimate of the spatial and temporal variation of climate within Amazonia.

(a) Precipitation

It is acknowledged that precipitation is the most important meteorological variable in the Tropics and hence arguably the most important variable to model correctly for this type of study. A thorough assessment can be made of the validity of the spatial and temporal distribution of modelled precipitation using recently published detailed observations of precipitation over central and western tropical South America (Figueroa and Nobre 1990). Modelled precipitation is compared for the four seasons, southern summer (December, January and February), southern autumn (March, April and May) southern winter (June, July and August), and southern spring (September, October and November) and the year in Figure 2.

Southern Summer

The mean position of the South Atlantic Convergence Zone, situated in western Amazonia and central Brazil at this time of year, results in centres of high precipitation with a NW-SE orientation. The model captures the position of these centres extremely well, but magnitudes are overestimated. For example, the area of maximum precipitation centred at 9 S 58 W, has a central high of >1200mm compared with the observed >900mm and this area extends too far towards the east and south.

The precipitation maxima on the eastern slopes of the Andes Cordillera in Peru and Ecuador and western Colombia, caused by mechanical lifting of low-level winds by the mountain barriers, are not well simulated by the model.

Southern Autumn

The modelled highest precipitation regions (>900mm) agree fairly well with observations. These occur along the equator with two maxima, one along the Atlantic coast and the eastern portion of Amazonia and the other over western Amazonia. The modelled western maximum is too high, and the eastern maximum is too low, especially along the Atlantic coast and does not extend far enough west.

South of the maximum areas of rainfall at the equator, modelled precipitation falls off rapidly and agrees favourably with observations over Amazonia.

The modelled precipitation over western Colombia now agrees more closely with observations but probably due to the limitations of resolution does not delineate a separate maximum over this area.

Southern Winter

The region of maximum precipitation is now displaced even further north, centred at 66 W 3 N. The model broadly defines this area but is unable to depict a separate maximum in western Colombia (as in southern autumn) and the maximum (>1050mm) over the border region of Colombia, Brazil and Venezuela is not as extensive as observed. The decrease in rainfall south of the equator is much exaggerated by the model with totals falling to negligible amounts over Amazonia.

Southern Spring

The very high increase in precipitation over western Colombia is not as well simulated by the model as in the previous season. On the whole the model tends to present a much more noisy pattern of precipitation over northern South America compared with the smoother observed field, although precipitation magnitudes agree broadly. The model captures the reduction in intensity of the southern winter region of maximum precipitation over western Amazonia. The emergence of the NW-SE orientated band of precipitation from western Amazonia through central Brazil is also evident although this extends too far south. Minimum precipitation is simulated along the north-eastern Atlantic coast but totals appear to be a little too low.

Annual Total

The spatial distribution of the broad area of maximum precipitation over western Amazonia is well defined by the model but the magnitude is overestimated with values greater than the maximum 4000mm per year observed. On the north-eastern portion of this maximum, a steep gradient of rainfall in the Brazil-Venezuela-Guyana border region is well simulated by the model. Precipitation over central Amazonia is reasonably well represented by the model. The orographic rains in Peru and Ecuador are not captured by the model as noted for southern summer; however the model provides a better simulation over the mountainous regions of western Colombia.

In summary, the most significant features of simulated rainfall for this particular study are well captured by the model. The areas of maximum precipitation in western Amazonia are well positioned although magnitudes are a little too high. When the whole year is considered, the spatial distribution of rainfall is well simulated over a large proportion of central Amazonia but rainfall maxima are marginally overestimated during southern summer and underestimated during southern winter.

(b) Interception and Evaporation

Figure 1 compares monthly values of interception. There is a marked improvement in the simulation of interception, although the seasonality is exaggerated by the model, with consequently too little interception from May to September. This shortfall can be attributed to an underestimation in rainfall during these months. The annual mean value of 24mm now compares much more favourably with the measured value of 28mm.

Figure 3 shows monthly values of total evaporation. Although the proportion of interception to total evaporation has been improved (now 37% compared with a previous value of 71% for OC and the observed 25%), total evaporation appears to be too low. The largest shortfalls occur from June to November. This deficiency is again largely associated with a lack of rainfall during these months although the low evaporation may itself contribute towards too little rainfall.

(c) Net Surface Radiation, Surface Temperature and Top of the Atmosphere Net Radiation

Figures 4 and 5 show the seasonal variation of the surface net radiation and surface temperature for the model compared with observations. The model largely captures the seasonal cycle in net radiation but overestimates the magnitude by about 20%. Modelled surface temperature is underestimated by about 10%. Peak values from August to October are exaggerated by the model as a result of the excessive drying of the surface at this time of the year.

Figure 6 compares the modelled radiation at the top of the atmosphere for January and July with data from the Earth Radiation Budget Experiment (ERBE) (Barkstrom 1984) for January 1986 and July 1986 respectively. The model produces a good simulation of top of the atmosphere radiation for both months. Hence, as the radiation reaching the surface is overestimated this suggests that there is too little atmospheric attenuation by the model. One probable reason for this is the omission of aerosols which can absorb a significant proportion of radiation in the boundary layer.

(d) Runoff

Annual mean modelled runoff for the Amazon basin of 2.55×10^5 $m^3 s^{-1}$, (this value includes the Tocantins system of rivers), compares favourably with the observed 2.68×10^5 $m^3 s^{-1}$ (Vorosmarty et al. 1989); however, the seasonal distribution of runoff (not shown) is not captured by the model. This is primarily due to the definition of modelled basin runoff. At present basin runoff is calculated by assuming that local runoff reaches the mouth of the river instantaneously whereas in reality there can be a lag of several months. This time delay will be dependent on a number of factors not taken into account by the model, including topography, and the distributed nature of soil characteristics.

(e) Summary

In summary the performance of the new control simulation (NC) shows a substantial improvement in modelling interception compared with the old control experiment as presented in Lean and Warrilow (1989). We have demonstrated that the model can produce a fairly realistic simulation of precipitation both spatially and temporally. Area monthly averages of surface temperature and net surface radiation also provide adequate descriptions of single site measurements in central Amazonia. Simulated values of net radiation absorbed at the top of the atmosphere for South America compare favourably with observations. However, modelled total evaporation now appears to be deficient.

5. Deforested Experiment

In order to simulate the gross effects of total removal of the Amazonian forest all global boundary conditions were kept constant except over South America north of 30°S. Here all tropical forest and savannah were replaced by tropical pasture. Table 1 lists the vegetation parameters averaged over Region 1 (see Figure 7) for the control (NC) and deforested simulations (DF).

In summary, comparing the deforested with the control simulation, root depth (ie the average depth of soil from which moisture is available to plant roots) is reduced; albedo is increased (see Figure 7), as pasture reflects more solar radiation than forests which are very efficient absorbers and scatterers of short-wave radiation; surface resistance to evaporation is less for pasture under conditions of freely available soil moisture; roughness is reduced as forests offer a significant resistance to the wind in the lower layers of the atmosphere; the infiltration factor is larger for forests as tree root systems and forest litter enhance the infiltration rate. The change in soil parameters associated with the replacement of forest by pasture is little known due to a lack of observations. Hence in order to minimise the uncertainties introduced all soil characteristics were kept constant except the infiltration capacity which is dependent on the infiltration factor.

6. Results

In the following section we will present results from the three-year control (NC) and deforested (DF) simulations. The integrations were started at the end of June. All results are displayed for either South America or averaged over an area, Region 1 (see Figure 7) in which the imposed change in surface characteristics was a maximum. All tabulated results are averaged over the three years excluding the first month when the model is still adjusting to the boundary conditions.

(a) Seasonal Changes in Important Climatological Variables

Figure 8 shows the monthly mean values for a number of important climatological variables, for the control and deforested simulations and the change caused by deforestation.

Rainfall has decreased in almost every month throughout the three years, with the exception of four individual months when small increases are apparent, which can be attributed to natural climate variability. The decrease in rainfall ranges between 0.1 and 3mm day^{-1} with no seasonal bias.

There has been a marked reduction in evaporation in almost all months. The largest decreases occur when soil moisture limits evaporation - for typical soils in this region this occurs when soil moisture concentration falls below the critical value of 0.07. Figure 8(e) shows that in a deforested climate the surface layer is drier in this sense for a larger proportion of the year.

Monthly values of surface temperature have mostly increased, by between 1°C and 4°C throughout the three years. The change in temperature is a result of the new equilibrium that is established between the cooling caused by the reduction in net radiation absorbed at the surface (see section 6(c) later) and the warming caused by the reduction in evaporation. Most of the time the evaporative warming dominates; however, during the second and third July there are anomalous decreases in temperature, when reductions in surface radiation are high.

Total runoff shows increases and decreases which over the three years almost cancel leaving a small negative residual. In contrast surface runoff shows substantial increases during the three years, primarily as a result of the reduction in infiltration capacity. This is most apparent during the wet season in the first and the third years. In some months there is a small fall in surface runoff which implies that either the magnitude of rainfall is less or that rainfall is occurring in less intensive bursts.

(b) Seasonal and Spatial Changes in Rainfall

Figure 9 displays maps of the change in rainfall for each season and the year and highlights areas that are statistically significant at the 95% confidence level or above. In the following analysis only those results which are statistically significant will be considered. Figure 10 displays the associated velocity potential and divergent wind at 200mb for the control simulation and the difference between the deforested and the control simulation for the annual mean.

Southern Summer

There is an expansive area of reduced rainfall over central South America near 10 S 65 W. The largest reductions over this area represent a 40-50% shortfall in rainfall. Although the region is dominated by reduced rainfall, some areas experience significant increases in rainfall. The Andes, near 5-10°S is one such example, although it is difficult to give a quantitative estimate of the likely magnitude of change, as the control simulation substantially underestimates rainfall here. It is also interesting to note

that there are changes in rainfall outside the immediate area in which the land surface changes were imposed. These differences are most notable in eastern Brazil, where there are considerable reductions and increases in rainfall, which are comparable with differences within the perturbed area.

Southern Autumn

The area of maximum decrease in rainfall broadly coincides with the area of maximum precipitation at this time of year, being displaced slightly south of the equator. The largest reductions in rainfall represent a fall of 40% (or 4mm d^{-1}) and lie within the perturbed area. This area of reduced rainfall now extends into the Andes, in sharp contrast to the previous season. There are also widespread changes in rainfall over most of eastern Brazil; these show some similarity in pattern to southern summer with increases over much of the region but decreases over a large area centred on the Bahia province.

Southern Winter

Rainfall reductions are now concentrated over north-western South America and are again broadly linked to the area of greatest precipitation. Maximum reductions are much more severe at this time of the year with totals falling by up to 65% (or 6mm d^{-1}). Changes in rainfall over the rest of South America are mostly small decreases. However it is difficult to draw any meaningful conclusions about changes in the central Amazon basin as the model is unable to capture realistic totals here for the control simulation.

Southern Spring

There is an extensive area of significantly reduced rainfall which affects much of western Amazonia and parts of central South America. The maximum reductions in rainfall represent a 30% (or 4 mm d^{-1}) shortfall. Some increases in rainfall totals are also apparent, most notably in Ecuador and Colombia; however, maximum totals in these areas are not particularly well simulated by the model for the control.

Annual Mean

When the whole year is considered almost all of northern South America experiences reductions in rainfall. Over the degraded area, the largest reductions in rainfall are concentrated in north-western and central South America. Outside this area there are comparable reductions over much of eastern Brazil. There is only one small area within South America which shows a significant increase in rainfall and this is located in the southernmost part of eastern Brazil.

The area of reduced rainfall over central South America coincides with the region over which the largest changes in surface characteristics were imposed (see Figure 7). It is mainly the influence of the higher surface albedo that is expected to reduce rainfall, predominantly through changes in atmospheric circulation over South America (Charney 1975; Mylne and Rowntree 1992). Figures 10(a) and 10(b) indeed demonstrate that there is reduced divergence at upper levels implying less convergence at lower

levels and less ascent through the atmosphere. This in effect corroborates the Charney (1975) mechanism.

(c) Annual Changes in the Radiational Balance at the Surface

In Table 2 we consider the net radiation balance at the surface. The downward component of solar radiation reaching the surface has increased due to a reduction in the cloud amount. However, the effect of the imposed increase in surface albedo dominates, and so the net solar radiation absorbed at the surface is less. The decrease in cloud amount and atmospheric moisture in the lower layers of the atmosphere (not shown here) reduce the amount of longwave radiation that is absorbed by the atmosphere and re-radiated back to the surface. The reduction in net longwave radiation absorbed at the surface is enhanced to an even greater extent by higher surface temperatures. Overall the net radiation absorbed at the surface is less and tends to be largely influenced by the greater loss in longwave radiation. As a result of the decrease in net radiation absorbed at the surface, the turbulent exchange of heat and moisture between the surface and the atmosphere is diminished.

(d) Summary of Annual Changes in Important Climatological Variables

Table 3 summarises the results presented so far and includes average values of a number of other important atmospheric and surface variables. Deforestation has caused a depletion in all components of the moisture balance at the surface. There has also been a reduction in the convergence of moisture into the basin (estimated as the difference between the precipitation and the evaporation). Although surface pressure is less over the basin, relative to the adjacent ocean there has been little change, and therefore this has little impact on the moisture flux from the ocean. The reduction in cloud amount is consistent with less rainfall. The surface soil layer is now much drier mainly due to the imposed reduction in the water holding capacity. The drier surface restricts evaporation and so promotes a higher surface temperature. In turn this greater surface temperature allows more longwave cooling and so reduces the amount of net radiation absorbed at the surface. The horizontal wind has increased in response to a reduction in the drag coefficient due to the imposed decrease in roughness.

7. Discussion

In this paper we have put forward a more physically-based solution to the representation of interception from the forest canopy. Most importantly, we have demonstrated that the model captures a realistic description of the present-day climate of Amazonia. Potentially, this allows us to make a more confident statement concerning the simulated characteristics of the climate following large-scale removal of the forest. In the context of this present study if we are to substantiate our findings here then we must

provide plausible physical explanations for the changes seen.

The key to understanding the complex interactions which occur between the forest and atmosphere lies in appreciating that changes in any one of the hydrological components can set into motion a cycle of events. This is primarily due to the integral role that the forest plays in sustaining the moisture cycle. This has been verified from observational studies which have shown that at least half of the rainfall falling in the Amazon basin is evaporated or transpired back into the atmosphere and is then available for further rainfall events (Salati 1979).

Let us now consider the likely reasons for the changes in some of the most important variables.

(a) Evaporation

The mechanisms controlling changes in evaporation are primarily driven by the imposed changes in albedo, roughness and the depth of water available to plant roots. Increased albedo allows less absorption of the incoming solar radiation and hence, less available energy for latent heat exchanges.

The response of evaporation to reduced roughness is more complex. Some insight can be gained by examining the Penman-Monteith equation (Rowntree 1991). Under wet conditions when the surface resistance is zero, the evaporation loss resulting from interception is reduced as roughness decreases. When dry conditions prevail evaporation will only decrease if the surface resistance remains below a critical value, whilst above this value small increases in evaporation are expected. Hence it is extremely important to model the process of canopy wetting correctly. Results here indicate that evaporation is reduced in almost all months. The largest reductions in evaporation occur at the driest periods of the year, when evaporation will also be constrained by soil moisture availability.

At this point it is relevant to consider an earlier similar deforestation experiment carried out by Lean and Warrilow (1989). Results from their simulation predicted a more severe impact on local climate, with rainfall and evaporation reduced by 20% and 27% respectively, and surface temperature increased by 2.5°C. However, the rather crude treatment of the wetting of the canopy adopted in their experiment may have overemphasised the role of the change in roughness. This would result in unrealistically high reductions in evaporation and in turn would influence other components of the moisture and heat balance at the surface.

(b) Rainfall

Reduced evaporation implies that there will be a reduction in the net amount of water recycled into the atmosphere and hence less rainfall. If this were the only mechanism operating then temporal and spatial changes in rainfall could be simply correlated with the corresponding changes in evaporation. However, this picture is complicated by changes in the atmospheric circulation and in the moisture transport from the adjacent oceans.

Changes in the pattern of circulation are most clearly defined during the Southern Hemisphere

summer, when a heat low is firmly established over central Amazonia, and are readily explained by the Charney (1975) mechanism. The imposed increase in albedo together with the associated changes in long wave radiation leads to the basin becoming a net radiative heat sink. So, in order to maintain a thermal equilibrium there will be a compensatory increase in subsidence. This will tend to suppress ascent within the atmospheric column and by implication the convergence of moisture into the centre of the low pressure system near the surface. Reductions in the frictional drag as a result of reduced roughness will also tend to reduce moisture convergence (Sud et al. 1988).

In response to these highly complex mechanisms, changes in rainfall are variable both on a seasonal timescale and spatially throughout South America. Within the area in which the forest was removed there are widespread changes throughout the year which are statistically significant at the 95% confidence level or above. This area tends to be dominated by intense patches of reduced rainfall. The average reduction in rainfall amounts to some 14% of the total but rainfall totals at particular locations can fall by as much as two or three times the spatial average. The most severe deficits are felt during southern winter with up to 65% reductions locally.

Although reduced rainfall is certainly the dominant signal some areas do experience increases in rainfall. These tend to be located over the mountainous regions of Peru, Ecuador and Colombia. However, it is impossible to make a quantitative estimate of the likely change in rainfall as the model underestimates orographic rain.

As a result of the change in circulation pattern within South America, the impact of deforestation appears to extend well beyond the immediate area in which the forest was removed. For example during southern summer and autumn there are large fluctuations in rainfall over eastern Brazil, which are statistically significant and of comparable magnitude to changes within the perturbed area.

It is the highly non-uniform nature of rainfall modulation that could have the most serious consequences for the livelihood of the region. At present agricultural crops in Brazil are maintained by moisture exported from the Amazon basin (Marques et al. 1979). For these crops it is not the overall reduction in rainfall that is important but more the denial of rainfall at critical stages in their development. The regrowth of forest within the perturbed area and the survival of forest in outlying areas may also be threatened by a lengthening of the dry season together with less rainfall at other times of the year (Salati 1984).

(c) Temperature

The increase in the spatially averaged surface temperature is consistent with the reduction in the energy used in evaporating water at the canopy and soil surface and the imposed reduction in roughness. The decrease in aerodynamic roughness will reduce the efficiency of the turbulent transfer of energy from the surface so that a higher surface temperature is then needed to remove this excess of energy.

(d) Runoff

Surface runoff is controlled by changes in the spatial distribution and intensity of rainfall, and the infiltration capacity. In this case the imposed reduction in infiltration capacity dominates over the reduction in rainfall allowing higher surface runoff. However, the response in surface runoff is highly dependent upon the formulation employed. For example in the earlier deforestation experiment by Lean and Warrilow (1989) surface runoff was seen to decrease, as higher reductions in rainfall counteracted the reduction in infiltration capacity. This highlights the difficult nature of the problem in hand as it is not possible to verify the treatment of runoff or the values chosen for infiltration capacities against observations.

(e) Summary

Until we are able to directly compare GCM predictions with actual measurements it is not appropriate to present these results as predictions of a future deforested climate. Also, because of the high levels of natural climate variablity in tropical locations it has not been possible to establish the implications for global climate during only three simulated years. However, the merit of this and other such experiments should not be underestimated as they have provided substantial insight into the complex interactions occurring between the atmosphere and surface following forest removal.

We have also been able to substantiate the powerful use to which both micrometeorological data and satellite-based data can be put. In the future, observation programs will provide an even greater potential for GCM modellers not only to improve physical parametrizations but also to more confidently simulate deforestation. One such current example is the joint Anglo-Brazilian Amazonian Climate Observation Study (personal communication Wright 1990; Shuttleworth et al. 1992); the aim of this project is to provide quantitative measurements of differences in land surface characteristics for large adjacent areas of cleared and uncleared forest at three sites across the Amazon basin. These will allow us to adopt a more precise methodology in which agreed scenarios for the imposed changes are run concurrently in different GCMs.

Table 1 Vegetation and soil parameters for the control (NC) and deforested (DF) simulations averaged over region 1.

Vegetation Parameter	NC	DF
Rootdepth (cm)	127.4	61.9
Albedo	0.136	0.188
Surface Resistance (s m^{-1})	119.7	82.2
Roughness (m)	0.79	0.04
Canopy Capacity (mm)	0.682	0.633
Vegetation Fraction	0.93	0.84
Infiltration Factor	5.00	1.93

Soil Parameter	NC & DF
SMC* at Wilting Point	0.143
SMC* at Critical Point	0.210
SMC* at Field Capacity	0.345
SMC* at Saturation	0.475
Exponent in Soil Conductivity Relationship	0.951
Saturated Conductivity for Soil Moisture Flow (cm s^{-1})	1.111x 10^{-4}
Volumetric Heat Capacity (J m^{-3} K^{-1})	2.549x 10^{+6}
Thermal Conductivity (J m^{-1} K^{-1} s^{-1})	0.603

* Soil Moisture Concentration

Table 2 Radiation balance at the surface for the deforested (DF) and control (NC) simulations and the difference between the two simulations (DF-NC) for 3 year means averaged over region 1.

Radiation Variable ($W\ m^{-2}$)	NC	DF	DF-NC
Solar Downward Component	220.00	228.59	8.59
Solar Upward Component	26.23	38.23	12.0
Net Solar	193.77	190.36	-3.4
Longwave Downward Component	397.11	395.78	-1.3
Longwave Upward Component	449.63	463.34	13.7
Net Longwave	-52.52	-67.56	-15.0
Net Surface Radiation	141.25	122.80	-18.5

Table 3 Selected climatological variables for the deforested (DF) and control (NC) simulations, and the % difference between the two simulations (DF-NC) for 3 year means averaged over region 1.

Climatological Variable	NC	DF	DF-NC
Total Evaporation (E) (mm d^{-1})	2.28	1.73	-24%
Interception (mm d^{-1})	0.77	0.69	-10%
Precipitation (P) (mm d^{-1})	5.69	4.88	-14%
Moisture Convergence (P-E) (mm d^{-1})	3.41	3.15	-8%
Soil Moisture (cm)	13.422	4.63	-65%
Total Runoff (mm d^{-1})	3.34	3.14	-6%
Surface Runoff (mm d^{-1})	1.72	2.19	+27%
Cloud Amount (fraction)	0.59	0.55	-7%
Net Radiation (W m^{-2})	141.25	122.80	-13%
Surface Temperature (°C)	25.0	26.93	+1.9°C
Sensible Heat (W m^{-2})	75.33	72.44	-4%
Horizontal wind for bottom model level (m s^{-1})	2.36	3.39	+43.6%
Surface Pressure (mb)	1008.35	1007.96	-0.4mb

References

Barkstrom, B.R., The Earth Radiation Budget Experiment (ERBE). Bull. Am. Met. Soc., 65, 1170-1185. (1984)

Charney, J.G., Dynamics of Deserts and Drought in the Sahel. Quart. J. R. Met. Soc., 101, 193-202. (1975)

Dickinson, R.E. and Kennedy, P.J., Land Surface Hydrology in a General Circulation Model N-Global and Regional Fields Needed for Validation. Surveys in Geophysics 12, 115-126. (1991)

Dickinson, R.E., Implications of Tropical Deforestation for Climate- a Comparison of Model and Observational Descriptions of Surface Energy and Hydrological Balance. Philos. Trans. R. Soc. London B, 324, 423-431 (1989)

Dickinson, R.E., and Henderson-Sellers, A., Modelling Tropical Deforestation: A Study of GCM Land Surface Parametrizations. Q.J.R. Meteorol.Soc., 114, 439-462. (1988)

Dolman, A.J. and Gregory, D., The Parametrization of Rainfall Interception in GCMs, accepted for publication in Q.J.R. Meteorol.Soc. (1992)

Eagleson, P.S. and Qinliang, W., Moments of Catchment Storm Area, Water Resources Research, 21, 1185-1194. (1985)

Fearnside, P.M., Deforestation in Brazilian Amazonia. In G.M. Woodwell, ed., The Earth in Transition: Patterns and Processes of Biotic Impoverishment, 211-238, Cambridge University Press, New York. (1990)

Figueroa, S.N. and Nobre, C.A., Precipitation Distribution over Central and Western Tropical South America. Climanalise, 5, no.6, 36-45. (1990)

Gregory, D. and Rowntree, P.R., A Mass Flux Convection Scheme with Representation of Cloud Ensemble Characteristics and Stability Dependent Closure. Monthly Weather Review, 118, 1483-1506. (1990)

Lean, J. and Warrilow, D.A., Simulation of the Regional Climatic Impact of Amazon Deforestation. Nature, 342, 411-413. (1989)

Lloyd, C.R., Gash, J.H.C., and Shuttleworth, W.J., The Measurement and Modelling of Rainfall Interception by Amazonian Rainforest. Agricultural and Forest Meteorology, 43 277-294. (1988)

Marques, J., Santos, J.M., and Salati, E., O Campo do Fluxo de Vapor d'Agua Atmosferico Sobre a Regiao Amazonica. Acta Amazonica 9, no. 4, 701-713. (1979)

Mylne, M.F. and Rowntree, P.R., Deforestation of Amazonia- modelling the effects of albedo change. Accepted for publication in Climatic Change. (1992)

NOAA, National Climatic Center, World Weather Watch Records 1961-1970, 3, West Indies, South and Central America, NOAA, National Climatic Center, Asheville, N.C. (1982)

Rowntree, P.R., Atmospheric Parametrization Schemes for Evaporation over Land: Basic Concepts and Climate Modelling Aspects. In Schmugge, T.J. and Andre, A. J-C., eds., Land Surface Evaporation, Measurement and Parametrization, 5-29, Springer-Verlag New York, Inc., USA. (1991)

Salati, E, Victoria, R.L., Martinelli, L.A., and Richey, J.E., Deforestation and its Role in Possible Changes in the Brazilian Amazon. In Defries, R.S and Malone, T.F., eds., Global Change and our Common Future- Papers from a Forum, National Academy Press, 2101 Constitution Avenue, NW, Washington, DC 20418. 159-171. (1989)

Salati, E. and Vose, P.B., Amazon Basin: A System in Equilibrium. Science, 225, 129-138. (1984)

Salati, E., Dall Ollio. A., Gat, J., and Matsui, E., Recycling of Water in the Amazon Basin: an Isotope Study. Water Resources Research 15: 1250-1258. (1979)

Shukla, J., Nobre, C., and Sellers, P., Amazon Defrorestation and Climate Change. Science 247, 1322-1325. (1990)

Shuttleworth, W.J., Gash, J.H.C., Roberts, J.M., Nobre, C.A., Molion, L.C.B., and Ribeiro, M.N.G., Post-Deforestation Amazonian Climate: Anglo-Brazilian Research to Improve Prediction. (Accepted by Journal of Hydrology) (1992)

Shuttleworth, W.J. and Dickinson, R.E., Comments on 'Modelling Tropical Deforestation: A study of GCM Land-Surface Parametrizations', by R.E. Dickinson and A. Henderson_Sellers, Q.J.R. Meterol. Soc., 115, 1177-1179. (1989).

Shuttleworth, W.J., Evaporation from Amazonian Rainforest. Proc. R. Soc. London Ser. B, 233, 321-346. (1988a)

Shuttleworth, W.J., Macrohydrology- the New Challenge for Process Hydrology. Journal of Hydrology, 100, 31-56. (1988b)

Shuttleworth, W.J. and Calder,I.R., Has the Priestley-Taylor equation any relevance to forest evaporation? Journal of Applied Meteorology, 18, 639-646. (1979)

Slingo, A., Wilderspin, R.C., and Smith, R.N.B., The Effect of Improved Physical Parametrizations on Simulations of Cloudiness and the Earth's Radiation Budget in the Tropics. J. Geophys. Res. 94, 2281-2301. (1989)

Smith, R.N.B., A Scheme for Predicting Layer Cloud and their Water Content in a General Circulation Model. Q. J. R. Meteorol. Soc., 116, 435-460. (1990)

Sud, Y. C., Shukla, J. and Mintz, Y., Influence of Land Surface Roughness on Atmospheric Circulation and Precipitation: A Sensitivity Study with a General Circulation Model. Journal of Applied Meteorology, 27, 1036-1054. (1988)

Vorosmarty, C.J., Moore, B., Grace, A.L., Gildea, M.P., Melillo, J.M., Peterson, B.J., Rastetter, E.B., and Steudler, P.A., Continental Scale Models of Water Balance and Fluvial Transport: An Application to South America, Global Biogeochemical Cycles, 3, no. 3 241-265. (1989)

Warrilow, D.A. and Buckley, E., The Effect of Land Surface Processes on the Moisture Budget of a Climate Model. E Annales Geophysicae 7, No.5, 439-449. (1989)

Warrilow, D.A., Sangster, A.B., and Slingo, A., Modelling of Land Surface Processes and their Influence on European Climate, Met O 20 DCTN 38, Meteorological Office, Bracknell. (1986)

Wilson, M.F. and Henderson-Sellers, A., A Global Archive of Land Cover and Soils Data for Use in General Circulation Models, Journal of Climatology, 5, 119-143. (1985)

Figure Captions

Figure 1 Simulated monthly mean interception (mm $month^{-1}$) averaged over the region under consideration. Observations are from Shuttleworth (1988a).

Figure 2(a) Simulated precipitation pattern of the control experiment (NC) over South America for Southern Hemisphere summer (December, January, February) averaged over the 3 years. Contours are at 0, 30, 60, 150, 450, 600, 750, 900, 1050, 1200 then every 300 mm $month^{-1}$.

(b) Observed precipitation pattern over South America (Figueroa and Nobre, 1990) for Southern Hemisphere summer (December, January, February). Contours as for (a)

(c) As for (a) but for Southern Hemisphere autumn (March, April, May).

(d) As for (b) but for Southern Hemisphere autumn (March, April, May).

(e) As for (a) but for Southern Hemisphere winter (June, July, August).

(f) As for (b) but for Southern Hemisphere winter (June, July, August).

(g) As for (a) but for Southern Hemisphere spring (September, October, November).

(h) As for (b) but for Southern Hemisphere spring (September, October, November).

(i) As for (a) but for the year. Contours are at every 500mm $year^{-1}$.

(j) As for (b) but for the year. Contours are at every 500mm $year^{-1}$.

Figure 3 Simulated monthly mean evaporation (mm $month^{-1}$) averaged over the region under consideration. Observations are from Shuttleworth (1988a).

Figure 4 Simulated monthly mean net surface radiation (mm $month^{-1}$) (multiply by 0.96 to convert to Wm^{-2}) averaged over the region under consideration. Solid line represents the new control simulation (NC), dashed line the observations (Shuttleworth, 1988a).

Figure 5 Simulated monthly mean net surface temperature (°C) averaged over the region under consideration. Solid line represents the new control simulation (NC), dashed line the observations (NOAA, 1982).

Figure 6 (a) Simulated net radiation at the top of the atmosphere for the control experiment (NC) over South America for January averaged over the 3 years. Contours are at every 20 W m^{-2}.

(b) Observed ERBE net radiation at the top of the atmosphere over South America for January 1986. Contours are at every 20 W m^{-2}.

(c) As for (a) but for July.

(d) As for (b) but for July 1986.

Figure 7 Imposed change in albedo over South America. The box encompassed by the solid black line shows the area used for averaging purposes, Region 1; for all results quoted and signifies the largest change in land surface characteristics in the southern region.

Figure 8 (a) Simulated monthly mean rainfall (mm day^{-1}) averaged over the region under consideration. Solid line represents the deforested simulation (DF), dashed line the control simulation (NC).

(b) Simulated monthly mean difference of deforested (DF) minus control (NC) simulated rainfall (mm day^{-1}) averaged over the region under consideration.

(c) As for (a) but for evaporation.

(d) As for (b) but for evaporation.

(e) As for (a) but for soil moisture concentration (cm).

(f) As for (b) but for soil moisture concentration (cm).

(g) As for (a) but for surface temperature (°C).

(h) As for (b) but for surface temperature (°C).

(i) As for (a) but for total runoff.

(j) As for (b) but for total runoff.

(k) As for (b) but for surface runoff.

Figure 9 (a) Simulated change in precipitation pattern over South America due to deforestation for Southern Hemisphere summer (December, January, February) averaged over the 3 years. Contours are at 1mm day^{-1}, areas of decrease are stippled, and changes locally significant at the 95% confidence level or above are heavily shaded.

(b) As for (a) but for Southern Hemisphere autumn (March, April, May).

(c) As for (a) but for Southern Hemisphere winter (June, July, August).

(d) As for (a) but for Southern Hemisphere spring (September, October, November).

(e) As for (a) but for the year.

Figure 10 (a) Simulated velocity potential and divergent wind field at 200mb over South America for the year averaged over the 3 years. Contours are at every 0.5 x $10^6 m^2 s^{-1}$.

(b) Simulated change in velocity potential and divergent wind field at 200mb over South America due to deforestation for the year averaged over the 3 years. Contours are at every 0.5 x $10^6 m^2 s^{-1}$.

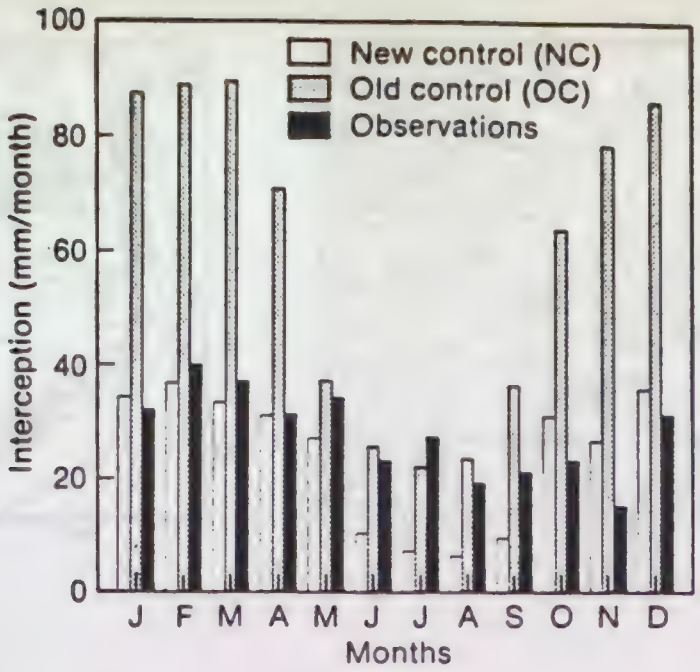

Figure 1

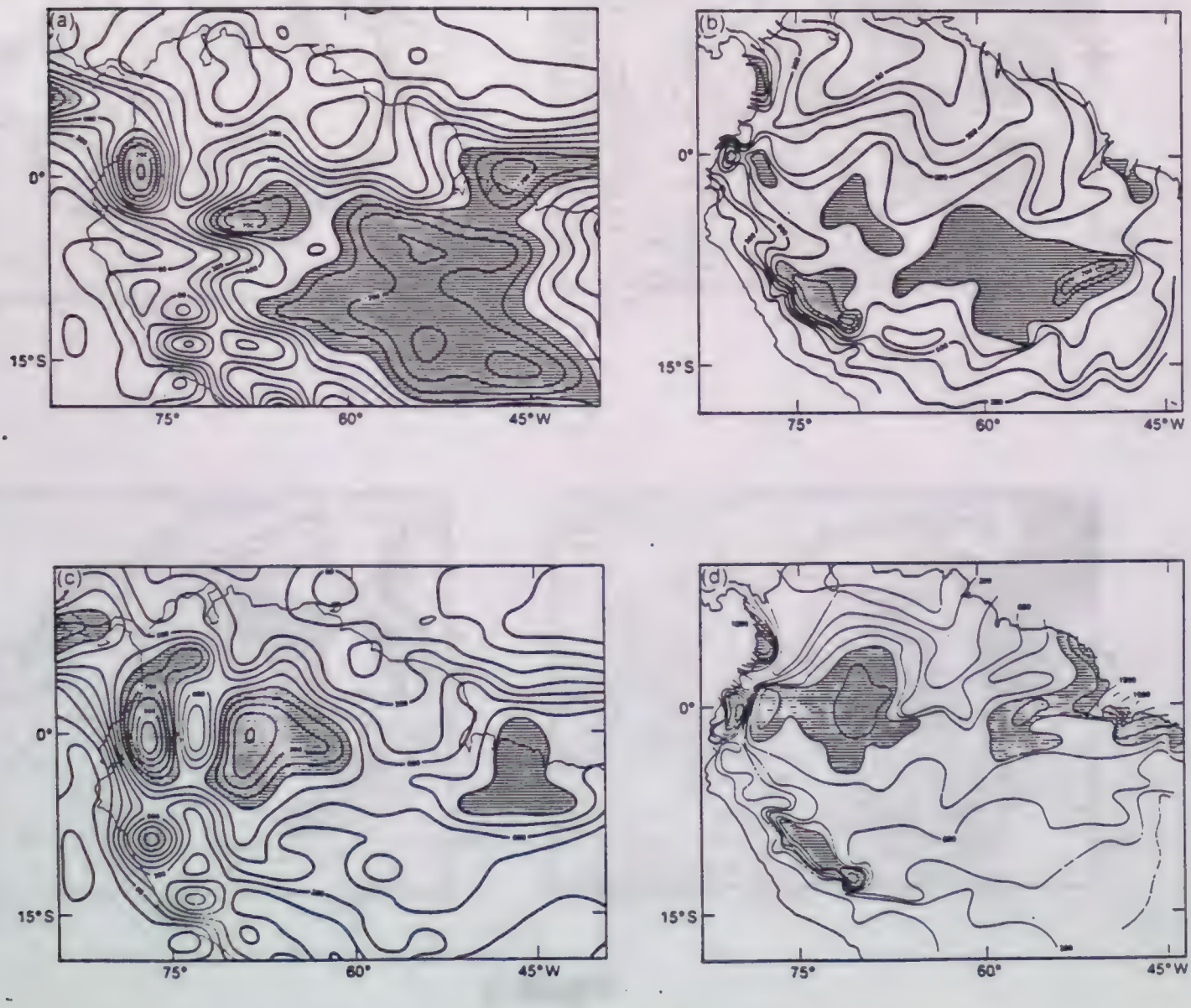

Figure 2

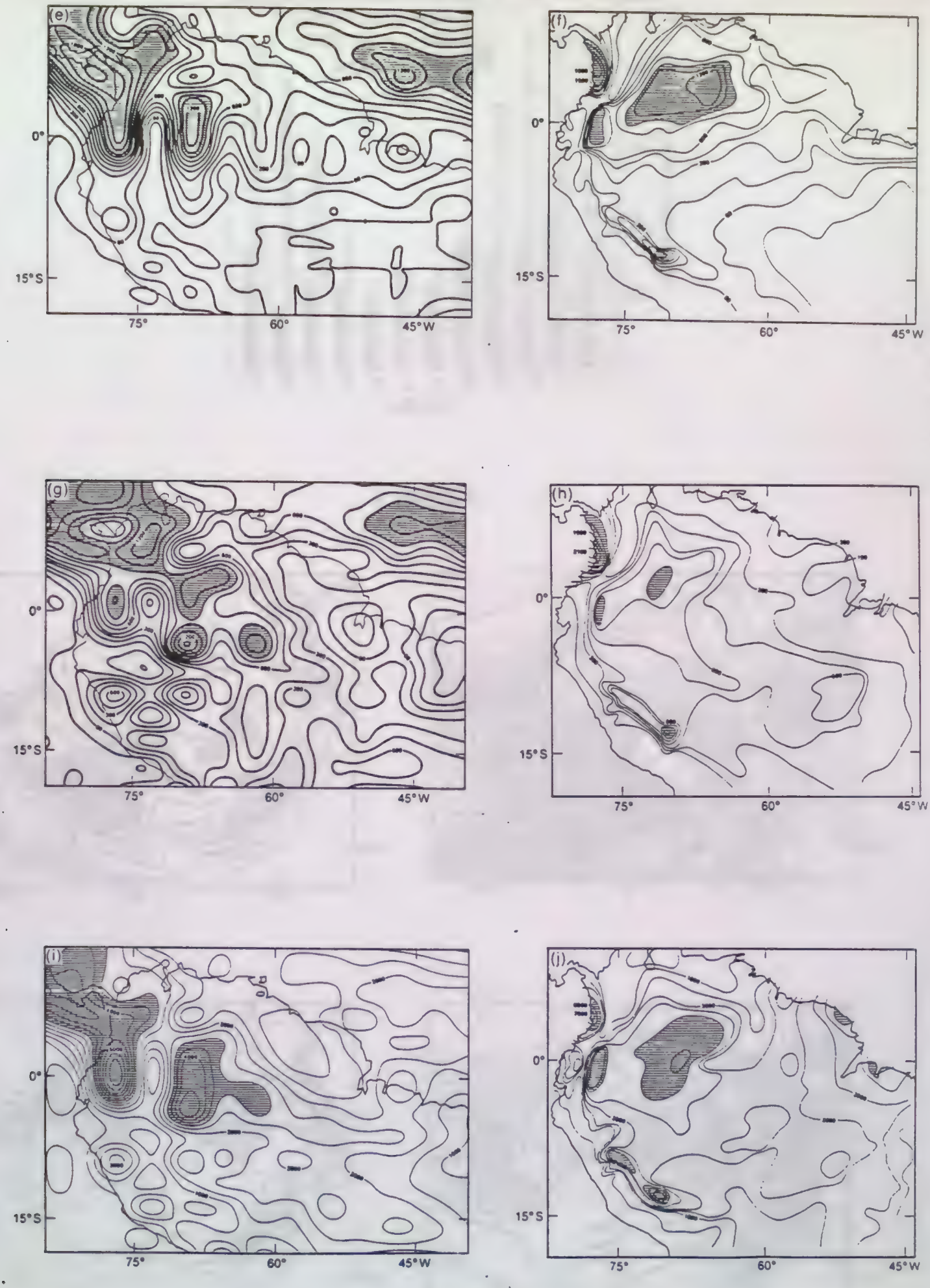

Figure 2

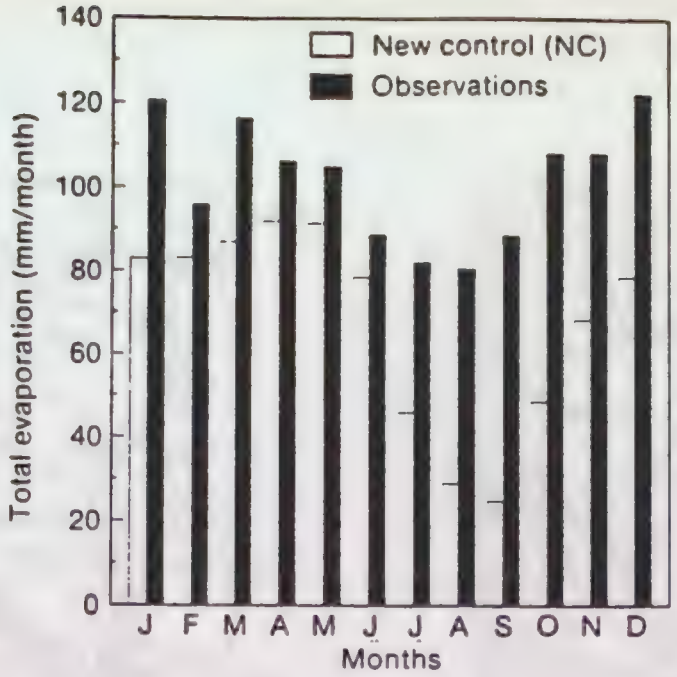

Figure 3

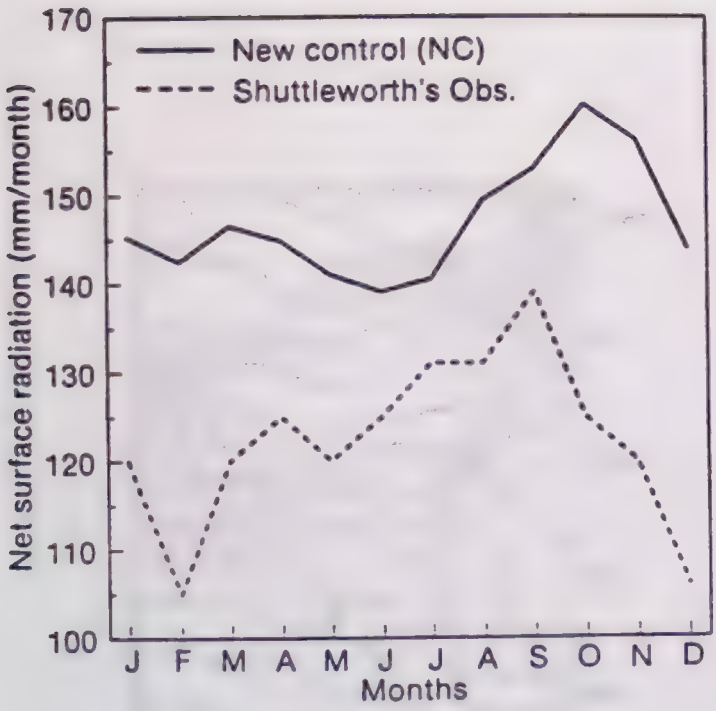

Figure 4

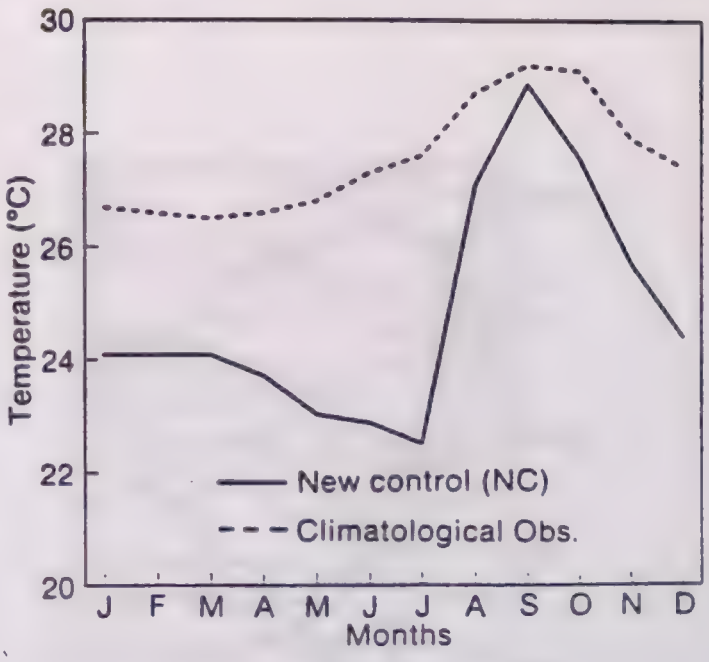

Figure 5

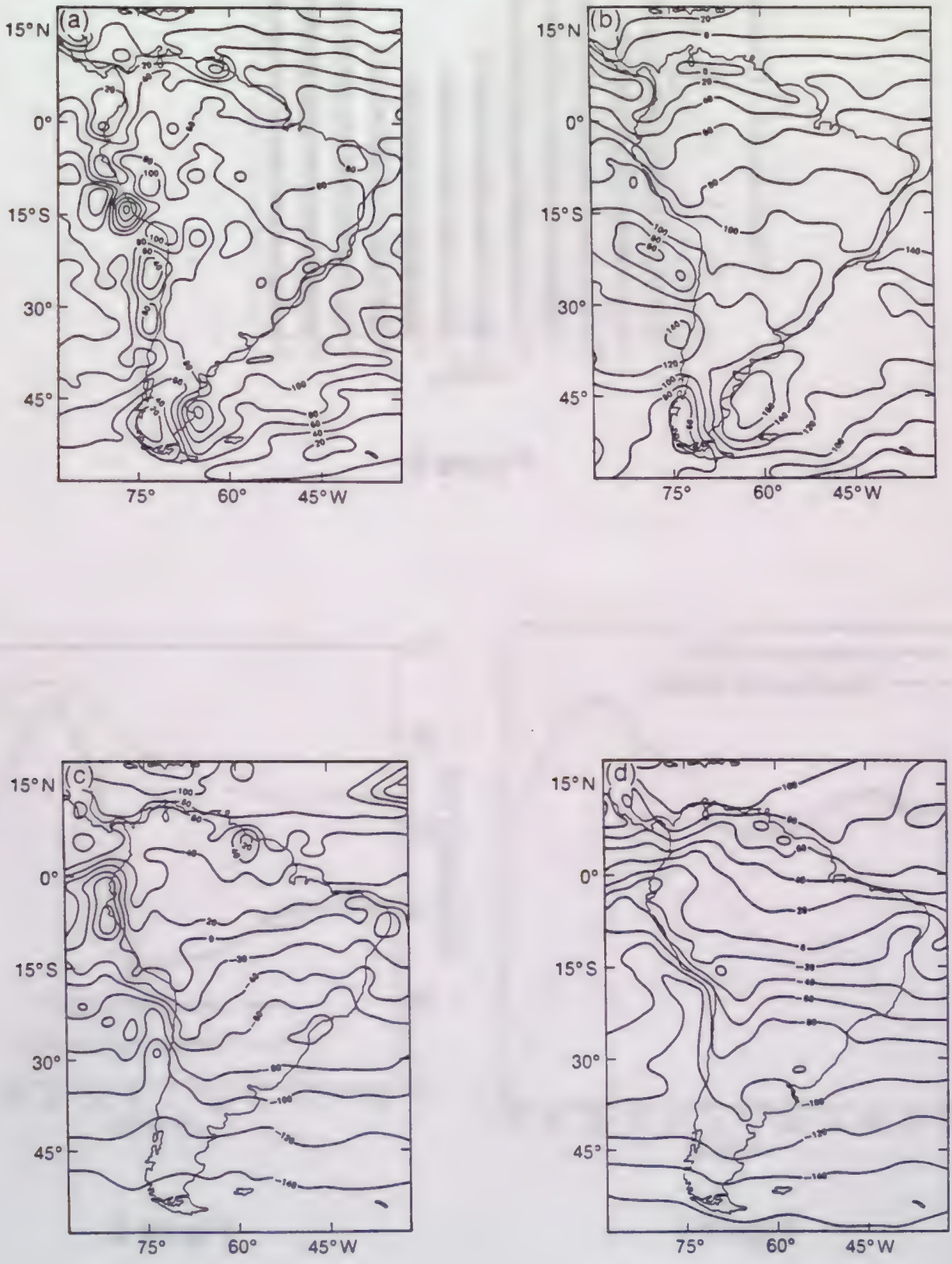

Figure 6

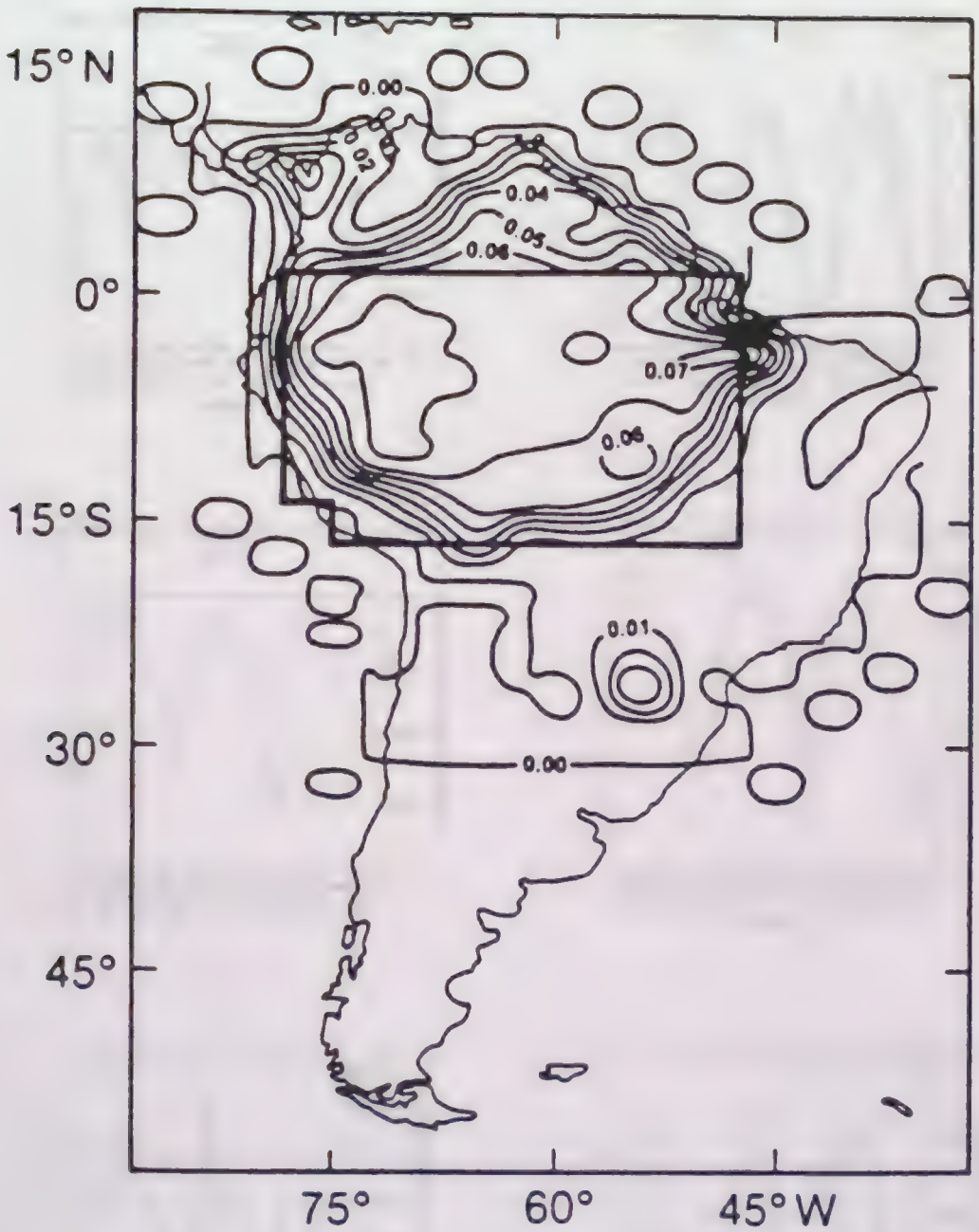

Figure 7

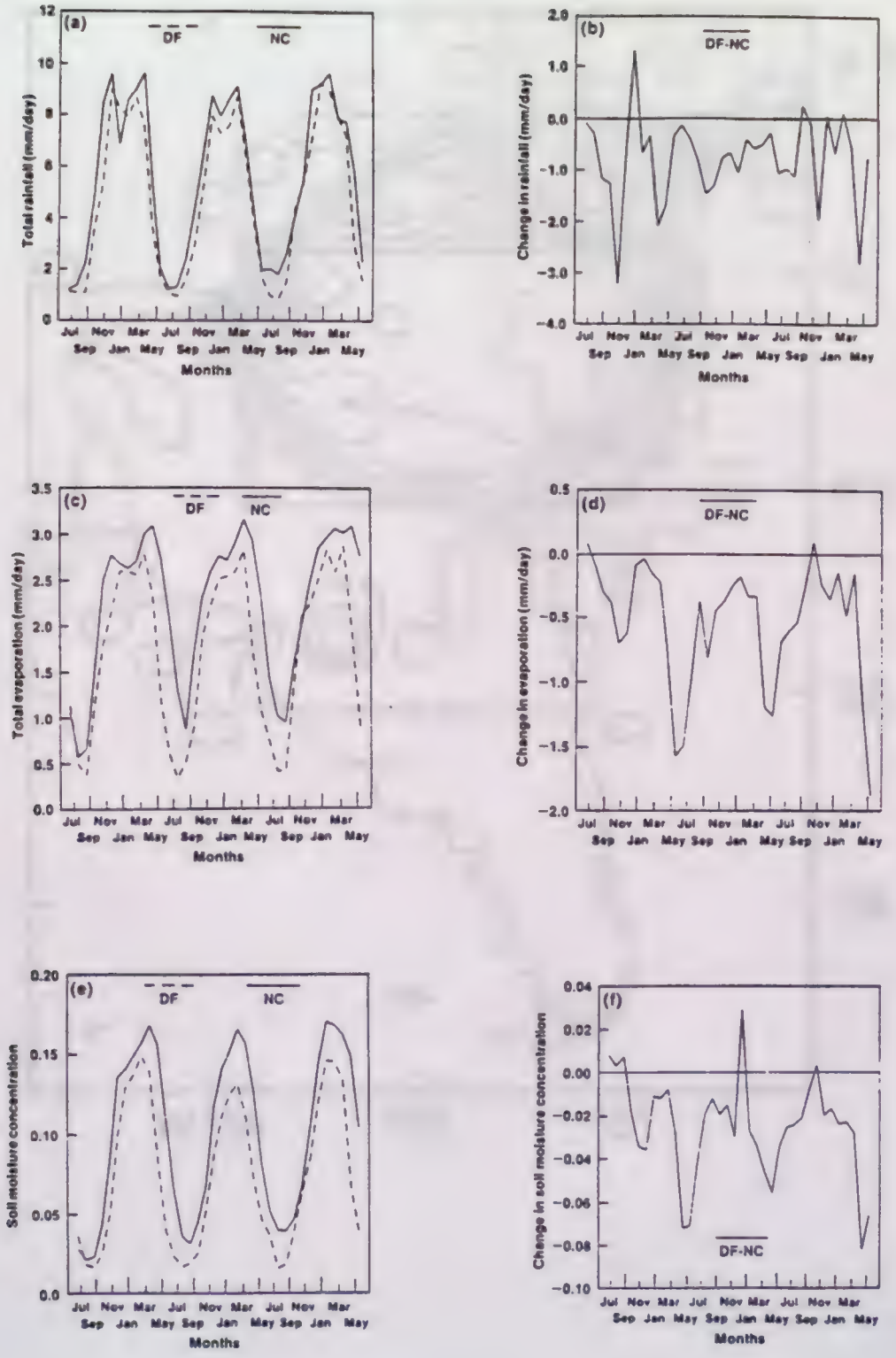
(a)
DF
NC
Total rainfall (mm/day)
12
10
8
6
4
2
0
Jul Nov Mar Jul Nov Mar Jul Nov Mar
Sep Jan May Sep Jan May Sep Jan May
Months
(b)
DF-NC
Change in rainfall (mm/day)
2.0
1.0
0.0
-1.0
-2.0
-3.0
-4.0
Jul Nov Mar Jul Nov Mar Jul Nov Mar
Sep Jan May Sep Jan May Sep Jan May
Months
(c)
DF
NC
Total evaporation (mm/day)
3.5
3.0
2.5
2.0
1.5
1.0
0.5
0.0
Jul Nov Mar Jul Nov Mar Jul Nov Mar
Sep Jan May Sep Jan May Sep Jan May
Months
(d)
DF-NC
Change in evaporation (mm/day)
0.5
0.0
-0.5
-1.0
-1.5
-2.0
Jul Nov Mar Jul Nov Mar Jul Nov Mar
Sep Jan May Sep Jan May Sep Jan May
(e)
DF
NC
Soil moisture concentration
0.20
0.15
0.10
0.05
0.0
Jul Nov Mar Jul Nov Mar Jul Nov Mar
Sep Jan May Sep Jan May Sep Jan May
Months
(f)
DF-NC
Change in soil moisture concentration
0.04
0.02
0.00
-0.02
-0.04
-0.06
-0.08
-0.10
Jul Nov Mar Jul Nov Mar Jul Nov Mar
Sep Jan May Sep Jan May Sep Jan May
Months

Figure 8

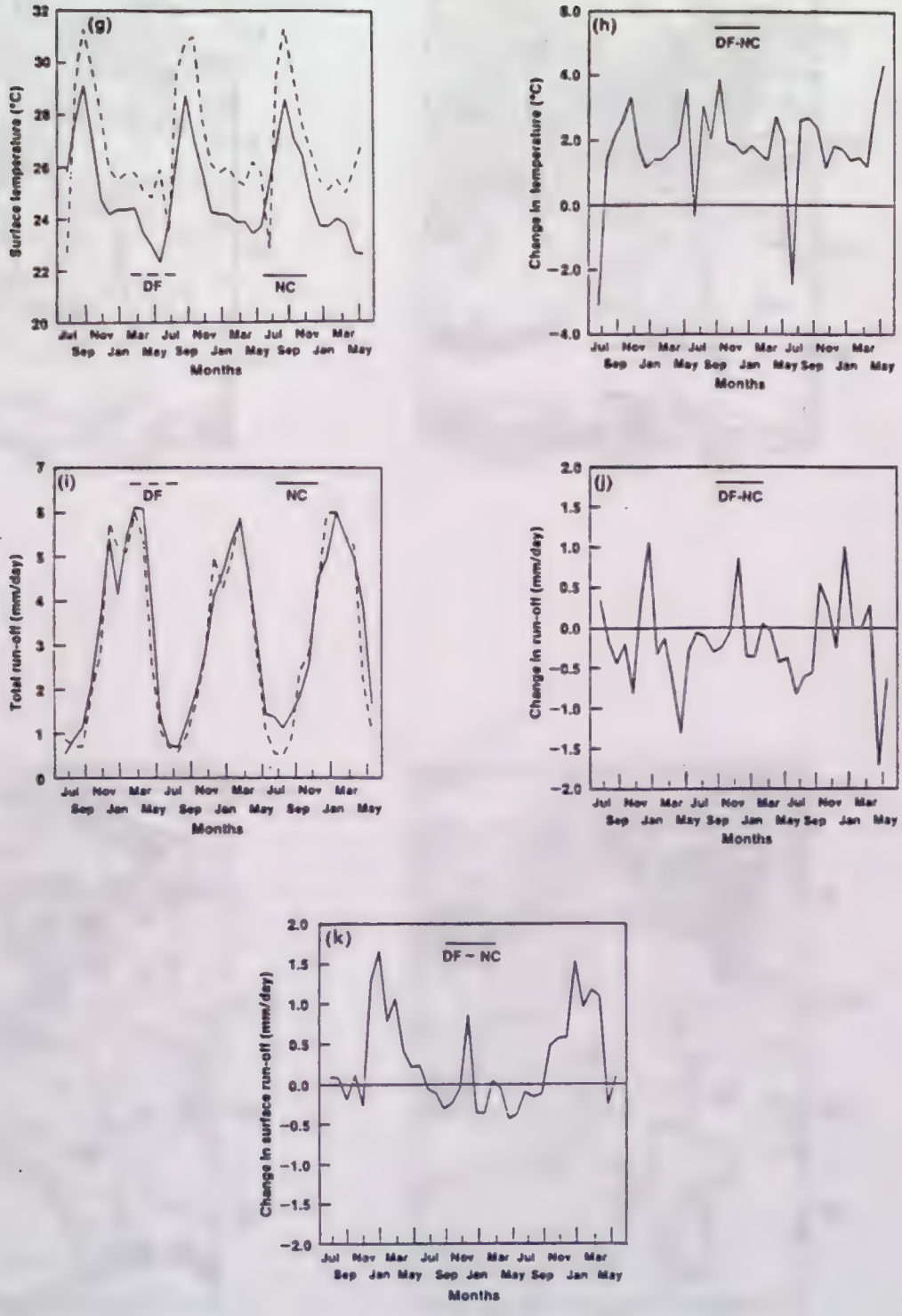
(g)
Surface temperature (°C)
DF
NC
(h)
DF-NC
Change in temperature (°C)
(i)
Total run-off (mm/day)
(j)
Change in run-off (mm/day)
(k)
DF − NC
Change in surface run-off (mm/day)
Jul Nov Mar Jul Nov Mar Jul Nov Mar
Sep Jan May Sep Jan May Sep Jan May
Months

Figure 8

Figure 9

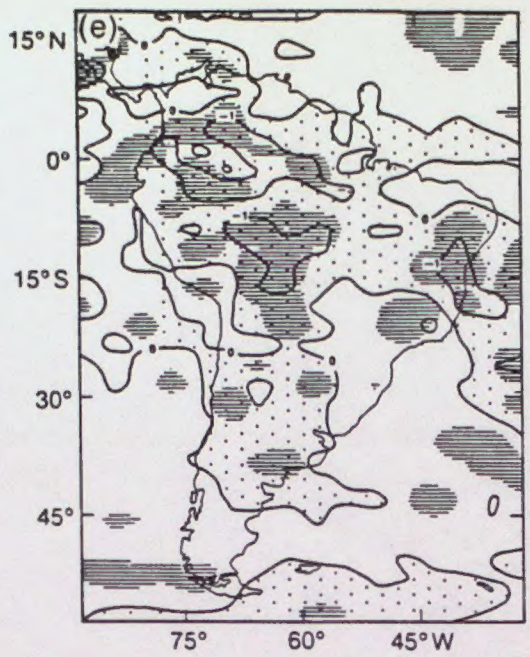

Figure 9

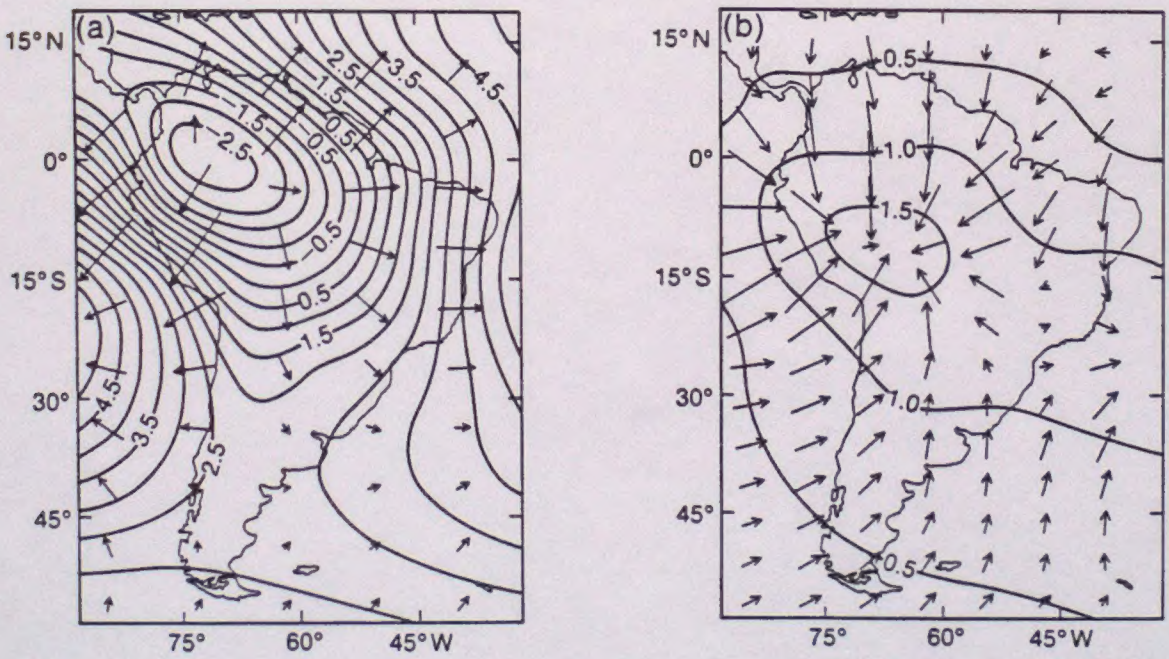

Figure 10

CLIMATE RESEARCH TECHNICAL NOTES

CRTN 1	Oct 1990	Estimates of the sensitivity of climate to vegetation changes using the Penman-Monteith equation. P R Rowntree
CRTN 2	Oct 1990	An ocean general circulation model of the Indian Ocean for hindcasting studies. D J Carrington
CRTN 3	Oct 1990	Simulation of the tropical diurnal cycle in a climate model. D P Rowell
CRTN 4	Oct 1990	Low frequency variability of the oceans. C K Folland, A Colman, D E Parker and A Bevan
CRTN 5	Dec 1990	A comparison of 11-level General Circulation Model Simulations with observations in the East Sahel. K Maskell
CRTN 6	Dec 1990	Climate Change Prediction. J F B Mitchell and Qing-cun Zeng
CRTN 7	Jan 1991	Deforestation of Amazonia - modelling the effects of albedo change. M F Mylne and P R Rowntree
CRTN 8	Jan 1991	The role of observations in climate prediction and research. D J Carson
CRTN 9	Mar 1991	The greenhouse effect and its likely consequences for climate change. D J Carson
CRTN 10	Apr 1991	Use of wind stresses from operational N.W.P. models to force an O.G.C.M. of the Indian Ocean. D J Carrington
CRTN 11	Jun 1991	A new daily Central England Temperature series, 1772-1991. D E Parker, T P Legg and C K Folland
CRTN 12	Jul 1991	Causes and predictability of Sahel rainfall variability. D P Rowell, C K Folland, K Maskell, J A Owen, M N Ward
CRTN 13	Jul 1991	Modelling changes in climate due to enhanced CO_2, the role of atmospheric dynamics, cloud and moisture. C A Senior, J F B Mitchell, H Le Treut and Z-X Li

CLIMATE RESEARCH TECHNICAL NOTES

CRTN 14	Sep 1991	Sea temperature bucket models used to correct historical SST data in the Meteorological Office. C K Folland
CRTN 15	Aug 1991	Modelling climate change, and some potential effects on agriculture in the U.K. P R Rowntree, B A Callander and J Cochrane
CRTN 16	Aug 1991	The Boreal Forests and Climate G Thomas and P R Rowntree
CRTN 17	Aug 1991	Development of a Stratosphere-Troposphere Data Assimilation System. R Swinbank.
CRTN 18	Sep 1991	A study of asynchronous coupling using a simple climate model. M K Davey.
CRTN 19	Sep 1991	The Oceanic Carbon Cycle. N K Taylor
CRTN 20	Nov 1991	Worldwide ocean-atmosphere surface fields in Sahel wet and dry years using provisionally corrected surface wind data. M N Ward
CRTN 21	Dec 1991	Coupled tropical ocean global atmosphere models at the UKMO. M K Davey, C Gordon, S Ineson and S Lawrence
CRTN 22	Dec 1991	Empirical parameterisation of tropical ocean-atmosphere coupling. M Allen, M K Davey, D L T Anderson and P D Killworth
CRTN 23	Feb 1992	The temporal evolution of Equatorial Currents in the Indian Ocean D L T Anderson, D J Carrington, R A Corry and C Gordon
CRTN 24	Feb 1992	Stratospheric analyses provided by the U.K. Meteorological Office M J Bailey, A O'Neill and V D Pope
CRTN 25	Feb 1992	Modelling interannual variability in the Indian Ocean using momentum fluxes from the UKMO and ECMWF operational weather analyses. D L T Anderson and D J Carrington